# Studies of ELM-mitigation with new active in-vessel saddle coils in ASDEX Upgrade

**W Suttrop, L Barrera, A Herrmann, R M McDermott, T Eich, R Fischer, B Kurzan, P T Lang, A Mlynek, T Pütterich, S K Rathgeber, M Rott, T Vierle, E Viezzer, M Willensdorfer[†], E Wolfrum, I Zammuto, and the ASDEX Upgrade Team**

Max-Planck-Institut für Plasmaphysik, EURATOM Association, D-85740 Garching, Germany

[†] Institut für Angewandte Physik, Technische Universität Wien, Association EURATOM-ÖAW, A-1040 Vienna, Austria

E-mail: suttrop@ipp.mpg.de

**Abstract.** The ASDEX Upgrade tokamak is currently being enhanced with a set of in-vessel saddle coils for non-axisymmetric perturbations aiming at mitigation or suppression of Edge Localised Modes (ELMs). Results obtained during the first experimental campaign are reported. With $n = 2$ magnetic perturbations, it is observed that type-I ELMs can be replaced by benign small ELM activity with strongly reduced energy loss from the confined plasma and power load to the divertor. No density reduction due to ELM mitigation (density "pump-out") is observed. ELM mitigation has, so far, been observed in plasmas with different shape, heating powers between a factor of $2-8$ above the H-mode threshold, different heating mixes and, therefore, different momentum input. The ELM mitigation regime can be accessed with resonant and non-resonant perturbation field configurations. The main threshold requirement appears to be a critical minimum plasma edge density which depends on plasma current. So far it is not possible to distinguish whether this is an edge collisionality threshold or a critical fraction of the Greenwald density limit.

PACS numbers: 28.52.-s, 52.55.Fa, 52.55.Rk

## 1. Introduction

Edge Localised Modes (ELMs) cause repetitive large energy outbursts from the main plasma which, extrapolated to ITER [1], likely lead to unacceptable first wall life time limitations due to fast wall materials erosion [2]. High priority research is directed towards mitigating ELM losses or even suppressing ELMs which seems possible by a range of techniques. The application of non-axisymmetric intentional error fields has earlier been found to affect ELMs in COMPASS-D [3]. The successful demonstration of complete ELM suppression in DIII-D at low [4] and ELM mitigation at high [5] edge collisionality has prompted the development of a magnetic perturbation coil arrangement suitable for ITER. Experiments at JET, NSTX and MAST have followed with different perturbation field configurations and

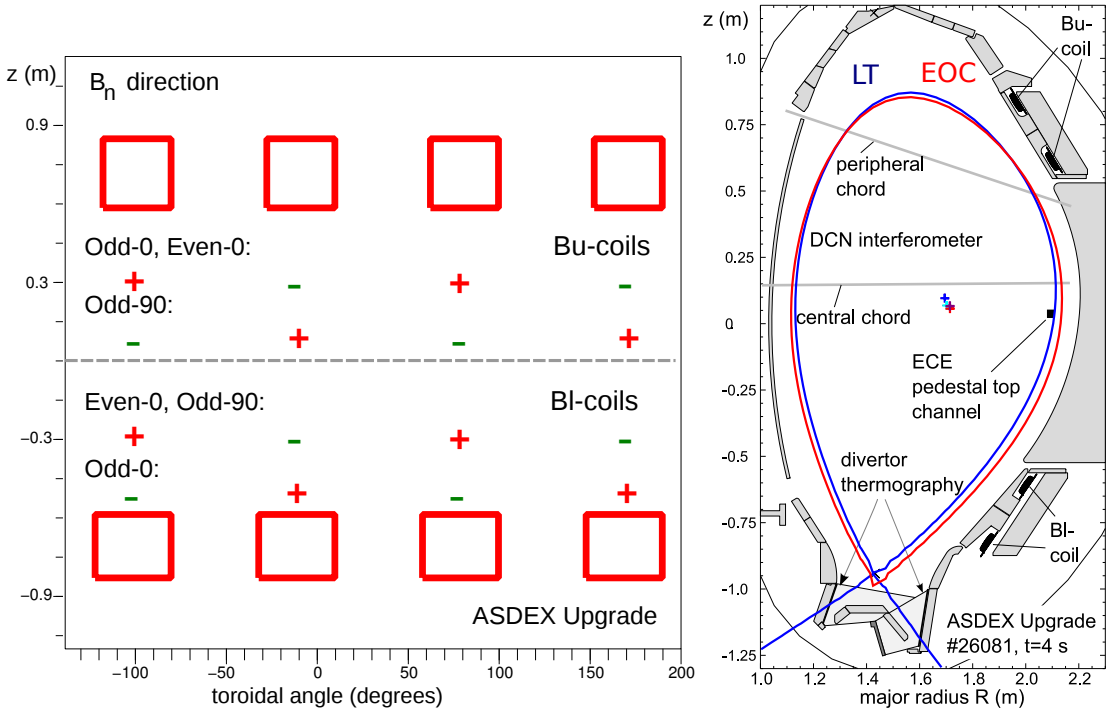


**Figure 1.** Arrangement of in-vessel saddle coils. Left: Toroidal position of coils and coil current configurations; Right: Poloidal section with plasma shapes LT and EOC.

different outcomes on ELM mitigation. The diversity of experimental results and the lack of a consistent extrapolation base for ITER so far have motivated the extension of ASDEX Upgrade with a set of ITER-like in-vessel saddle coils [6]. The first stage of this enhancement has quickly been found to be suitable for type-I ELM mitigation [7]. Experimental effort has since been directed to documenting the ELM mitigated regime, to broadening of the parameter range of existence, and to quantifying the access criteria.

## 2. Discharge behaviour with ELM mitigation

The first operating set of in-vessel saddle coils (dubbed "B-coils") in ASDEX Upgrade consists of two rows of coils above (Bu-coils) and below midplane (Bl-coils). Each row consists of four coils at different toroidal positions. The coils have one winding with five turns each. Fig. 1 shows the toroidal (left) and poloidal (right) coil positions. In this study, $n = 2$ perturbations are investigated, with same or opposite polarity of upper and lower coils, dubbed even or odd parity, respectively. For odd parity, both non-equivalent toroidal orientations, 0° and 90°, are probed. Coil current signs (positive sign denotes outward directed radial field in each coil) and short-hand notation for the various configurations are indicated in the left part of Fig. 1. As seen from the right part of the figure, the coils are close to the plasma boundary. Two main plasma shapes are used: a) low triangularity, $\delta_u = 0.11$ (LT) and an "edge-optimised" configuration (EOC) with $\delta_u = 0.13$ and plasma boundary conforming to the outer protection limiter shape.

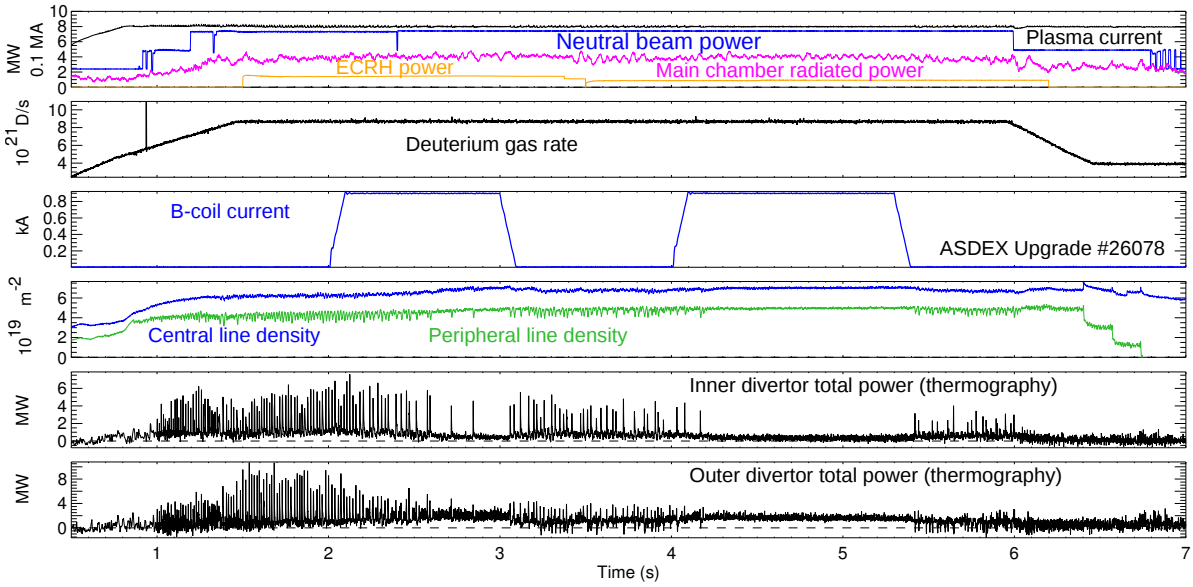


**Figure 2.** Time traces of H-mode discharge 26078 (LT, Odd-0) with ELM mitigation as in-vessel saddle coils (B-coils) are switched on.

Time traces of a typical discharge with ELM mitigation, shot 26078 (LT, Odd-0), toroidal field $B_t = -2.5$ T, plasma current $I_p = 0.8$ MA, edge safety factor $q_{95} = 5.6$, are shown in Fig. 2. A type-I ELMy discharge is set up with $P_{\mathrm{NBI}} = 7.5$ MW neutral beam heating, $P_{\mathrm{ECRH}} \leq 1.6$ MW central electron cyclotron resonance heating (ECRH) and a deuterium gas puff rate of $\Gamma_D = 9 \times 10^{21}$/s. An $n = 2$ perturbation (odd parity) is applied twice by ramping up the B-coil current to $I_{\mathrm{B-coil}} = 900$ A, corresponding to 4.5 kA$\times$turns. In the first B-coil pulse ($t = 2-3$ s), the frequency of type-I ELMs decreases gradually until they disappear. In the second pulse ($t = 4-5.5$ s), type-I ELMs vanish almost immediately after switching on the B-coils. In both cases, they re-appear when the coils are switched off. Apart from the presence of the perturbation field, a necessary condition for ELM mitigation appears to be that a minimum edge density is exceeded, which can be quantified as a line density of $5 \times 10^{19}$ m$^{-2}$ in the edge interferometer channel, corresponding to a line-averaged density of $\overline{n}_e = 6.5 \times 10^{19}$ m$^{-3}$.

The minimum density requirement is illustrated in Fig. 3 for discharge 26126 (LT, even parity). Here, the B-coils are on for the entire flat-top, but the transition from the type-I ELMy to the ELM-mitigated phase only occurs after a step of the gas puff rate from $\Gamma_D = 8.7 \times 10^{21}$/s to $9.7 \times 10^{21}$/s. All other parameters (plasma shape and position, heating power, etc.) are kept constant. The type-I ELMs become less frequent and interspersed with small transport events that cause minor oscillations of the plasma density (top trace). As type-I ELMs completely disappear above a peripheral line density of $5 \times 10^{19}$ m$^{-2}$, the density keeps rising and eventually saturates at $5.4 \times 10^{19}$ m$^{-2}$. At the same time the neutral density (shown in the second trace for the divertor) is not increasing. During the transition, in between type-I ELMs, the neutral density drops while the plasma density increases. This behaviour can be interpreted as an increased particle confinement in the ELM-mitigated phase

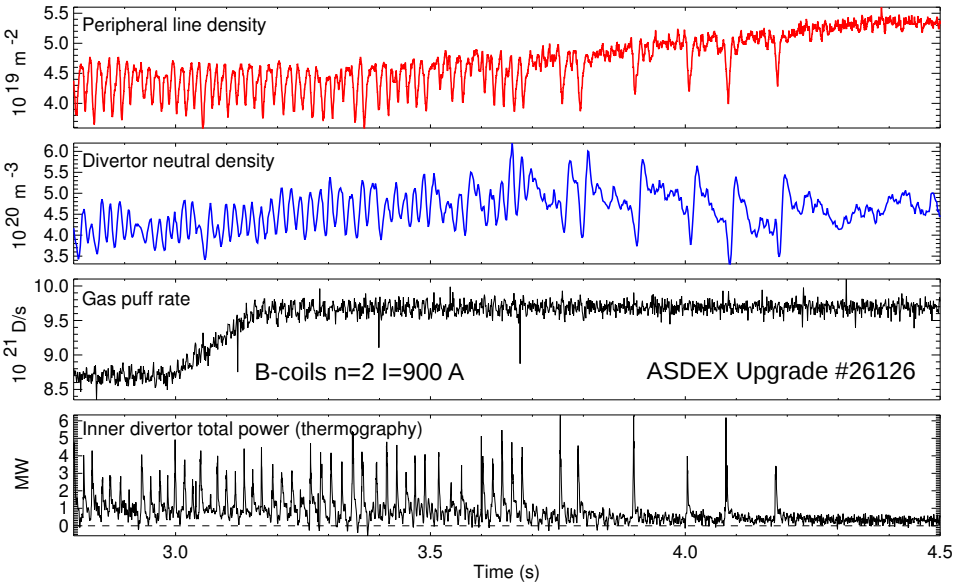


**Figure 3.** Transition phase to ELM mitigation induced by a step of the gas fueling rate.

compared to the average particle confinement in the type-I ELMy phase. It is interesting to note that nevertheless $Z_{\rm eff}$ is typically lower with ELM mitigation than without [8] and the core tungsten impurity concentration is also reduced [7].

## 3. Access conditions for ELM mitigation

It has been seen previously [7] that the ELM-mitigated regime can be accessed equally well with maximum resonant field (odd parity at $q_{95} = 5.4$) and non-resonant (i.e. minimum resonant) field (even parity). The resonant field component varies by a factor of 5.5; however, the measured coil current threshold for ELM mitigation is the same in both cases. Meanwhile, in several pairs of discharges odd and even parity configurations have been used with no apparent difference in plasma behaviour that could be attributed to the perturbation field configuration.

Access to ELM mitigation also seems to be independent of the plasma rotation which has been varied in Ref. [7] by varying the mix of neutral beam sources with different toroidal beam angle and therefore momentum input to the plasma, resulting in a toroidal velocity range of $30-40$ km/s at the pedestal top. Stronger reduction of momentum input is achieved by replacing a large fraction of neutral beam power with wave heating. Fig. 4 shows time traces of pulse 26895 (EOC, Odd-0, $I_p = 0.8$ MA, $B_t = -2.5$ T, $q_{95} = 5.5$) where until $t = 3.7$ s the plasma is heated with neutral beams, $P_{\rm NBI} = 7.5$ MW, injected in direction of the plasma current, and $P_{\rm ECRH} = 1.5$ MW central ECRH. From $t = 3.7-5.4$ s, the NBI power is reduced to $P_{\rm NBI} = 2.5$ MW, and complemented with ECRH, $P_{\rm ECRH} = 3.6$ MW, as well as ion cyclotron frequency heating (coupled power $P_{\rm ICRF} = 4.2$ MW, frequency $f_{\rm RF} = 36$ MHz). The total auxiliary heating power $P_{\rm aux}$, plasma density (interferometer edge channel) and MHD stored energy are comparable in both phases. While with B-coils off and NBI-dominated

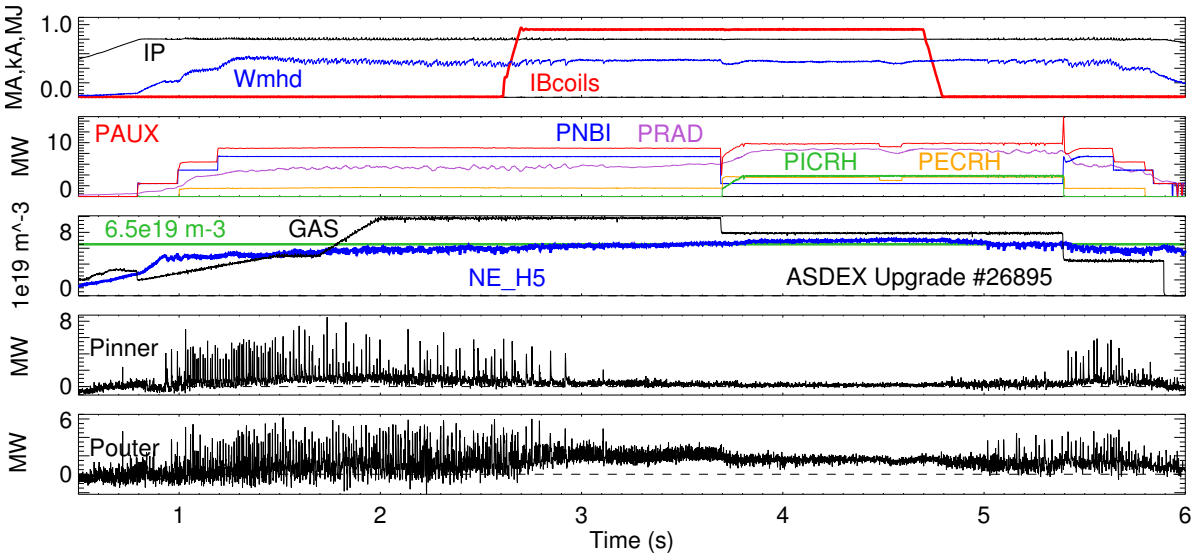


**Figure 4.** Comparison of NBI-dominated heating (until $t = 3.7$ s) with RF-dominated heating in pulse 26895 ($t = 3.7 - 5.4$ s)

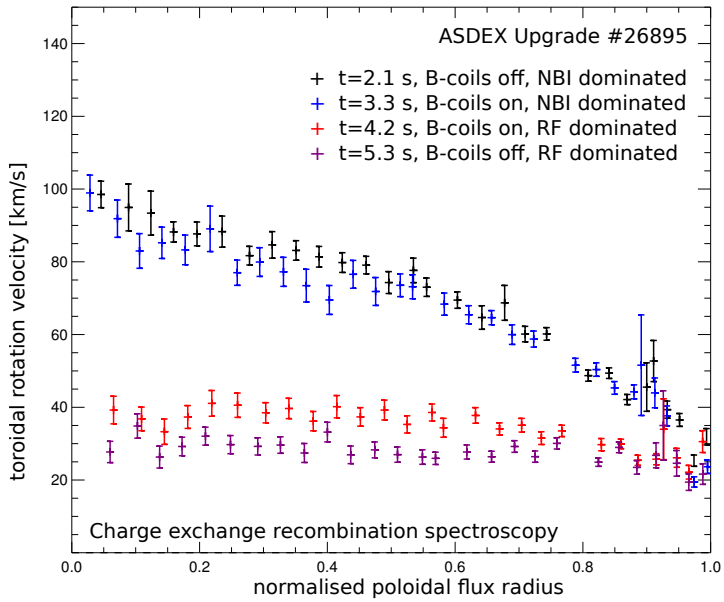


**Figure 5.** Toroidal rotation profiles measured by charge exchange recombination spectroscopy in pulse 26895.

heating, large type-I ELMs with peak divertor loads up to 8 MW (inner and outer divertor) prevail, combined heating with dominant RF power and with B-coils off ($t = 5 - 5.4$ s) is characterised by a mixture of type-I and small, type-III, ELM activity. In both cases application of perturbation fields ($t = 2.6 - 4.8$ s) leads to suppression of type-I ELMs, as seen most clearly from the reduced peak divertor power load.

Figure 5 shows profiles of the toroidal rotation velocity, measured by charge exchange recombination spectroscopy as a function of normalised poloidal flux radius $\rho_p \equiv [(\psi - \psi_{\mathrm{axis}})/(\psi_{\mathrm{boundary}} - \psi_{\mathrm{axis}})]^{1/2}$ ($\psi$: poloidal flux). The plasma core profiles $\rho_p \leq 0.9$ are

**Table 1.** Parameters of discharges with different plasma current and B-coil configurations as type-I ELM mitigation is reached (see text).

| Shot | shape | B-coils | $I_p$ (MA) | $t$ (s) | $\overline{n}_{\mathrm{e,edge}}$ $10^{19}$ m$^{-3}$ | $f_{\mathrm{GW}}$ | $T_i$ (eV) | $\nu_i^*$ |
|---|---|---|---|---|---|---|---|---|
| 26078 | LT | Odd-0 | 0.8 | 4.3 | 6.6 | 0.65 | 550 | 1.24 |
| 26126 | LT | Odd-0 | 0.8 | 6.64 | 6.7 | 0.66 | 620 | 1.0 |
| 26910 | EOC | Odd-0 | 0.8 | 4.7 | 6.7 | 0.67 | 480 | 1.61 |
| 26911 | EOC | Odd-90 | 0.8 | 4.06 | 6.6 | 0.65 | 450 | 1.79 |
| 26912 | EOC | Even-0 | 0.8 | 4.6 | 7.0 | 0.69 | 550 | 1.29 |
| 26956 | EOC | Odd-0 | 1.0 | 4.7 | 8.6 | 0.68 | 530 | 1.33 |
| 26987 | EOC | Odd-90 | 1.0 | 4.56 | 7.8 | 0.61 | 460 | 1.59 |
| 26990 | EOC | Odd-90 | 1.0 | 5.41 | 8.4 | 0.66 | 550 | 1.21 |

measured at the $C\,VI,\ n = 8 \rightarrow 7$ transition at $\lambda = 529.059$ nm; the edge profiles ($\rho_p \geq 0.9$) are measured with a separate spectrometer and viewing optics at the $B\,V,\ n = 7 \rightarrow 6$ transition ($\lambda = 494.467$ nm). The RF-dominated phase is characterised by a flattening of the rotation profile. The toroidal rotation at the position of the pressure pedestal top ($\rho = 0.95$) decreases from about 40 km/s (NBI-dominated heating) to 25 km/s (RF-dominated heating). The edge plasma rotation profile does not change significantly as the magnetic perturbation is applied. This is a general observation made so far in all H-mode plasmas with $n = 2$ perturbations.

Several shots with different plasma currents, $I_p$, different plasma shapes (LT or EOC) and different B-coil configurations have been made to investigate the density threshold for ELM mitigation. Shot parameters are listed in Table 1. In all these shots, the B-coil current is set to $I_{\mathrm{B-coil}} = 900$ A, well before the gas puff rate is ramped up to achieve ELM mitigation. The peripheral line-averaged density $\overline{n}_{\mathrm{e,edge}}$ (chord as shown in Fig. 1) and the ion temperature $T_i$ (from charge exchange spectroscopy) are taken in the mitigated phase after the last preceding type-I ELM; $T_i$ is taken at the position $\rho_p = 0.95$, as obtained from the axisymmetric equilibrium reconstruction. These measurements are selected for robustness and availability in each of these shots, and are not intended to replace detailed profile analysis, e.g. in [8]. The transition density depends clearly on the plasma current ($\overline{n}_{\mathrm{e,edge}} \sim 6.7 \times 10^{19}$ m$^{-3}$ at $I_p = 0.8$ MA; $\overline{n}_{\mathrm{e,edge}} \sim 7.8 - 8.6 \times 10^{19}$ m$^{-3}$ at $I_p = 1$ MA). However, there is little variation of the fraction $f_{\mathrm{GW}}$ of the Greenwald density [9]. The regime boundary might also be a collisionality requirement, as implied in Ref. [10]. Table 1 quotes the neoclassical ion collisionality $\nu_i^* \equiv \nu_{ii}(m_i/kT_i)^{1/2}\varepsilon^{-3/2}qR$, which is evaluated assuming $q = q_{95}$, $\varepsilon = 0.303$ and $Z_{\mathrm{eff}} = 1$. There is variation in $\nu^*$, however, no systematic dependence on $I_p$ or coil configuration.

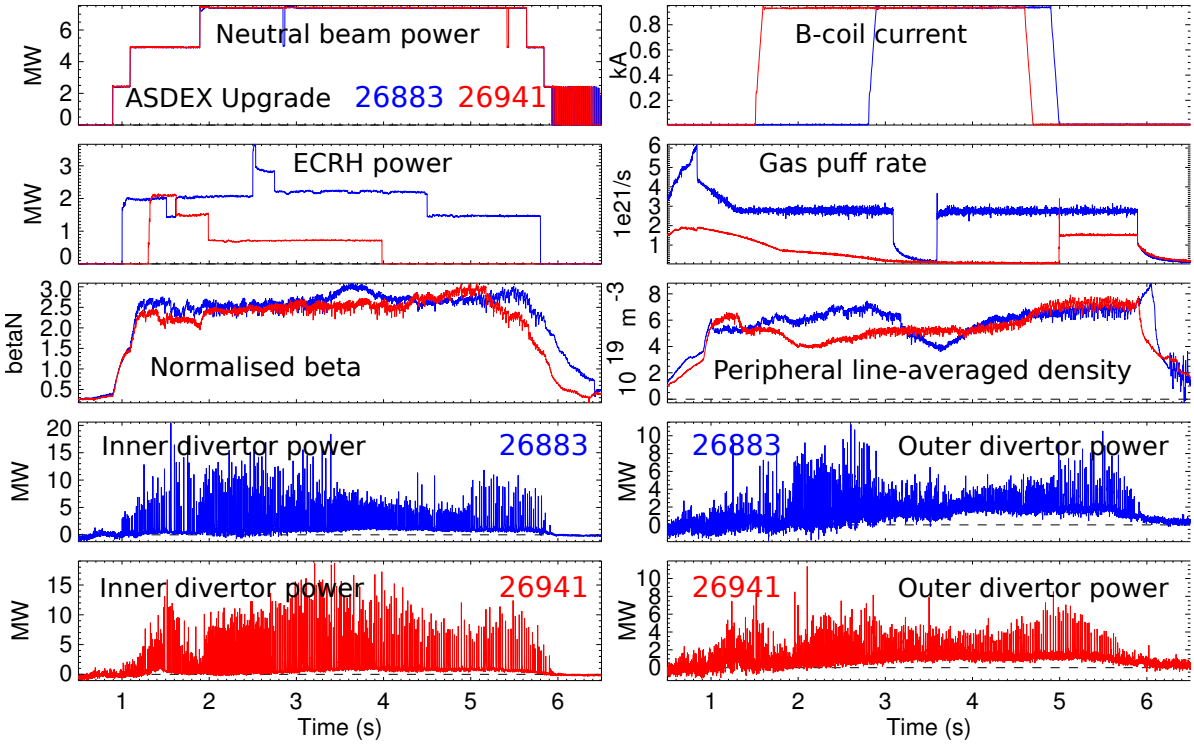


**Figure 6.** Time traces of plasmas aiming at low density and low safety factor: Pulse 26883 (blue lines, unboronised wall), pulse 26941 (red lines, fresh boronisation)

## 4. Search for a low density ELM mitigation regime

Initial experiments in ASDEX Upgrade have been performed which aim to establish a low collisionality, low safety factor ELM suppression regime such as the one described for DIII-D [10]. Figure 6 shows time traces of two discharges, pulse 26883 with unboronised plasma-facing components, and pulse 26941 after fresh boronisation. Both shots are at $B_t = -1.76$ T (third harmonic central ECRH), $I_p = 1$ MA, $q_{95} = 3.2$, with EOC shape and B-coils in Even-0 (resonant) configuration. The gas puff rate is kept as small as possible in both pulses, however, without wall conditioning (pulse 26883) there is only a short period entirely without gas puff ($t = 3.1 - 3.6$ s) in order to avoid density profile peaking and impurity accumulation. The edge ion collisionality is $\nu_i^* = 0.27, 0.14, 0.36$ for pulse 26883 at $t = 3.0$, $t = 3.6$ and pulse 26941, $t = 3.4$ s, respectively. Type-I ELMs prevail throughout these pulses, as they do in a reference discharge with B-coils off (26884, not shown). The main visible effect of the magnetic perturbation is the density drop in pulse 26941 at $t = 1.8$ s after the B-coils are switched on and the recovery of the density at $t = 4.7$ s as the coils are switched off.

## 5. Summary and Discussion

So far, ELM mitigation with $n = 2$ magnetic perturbations in ASDEX Upgrade is observed over a wide range of safety factors, $q_{95} = 4.5 - 6.5$, with different perturbation field configurations, but it appears to be limited to high density plasmas, $n \geq 0.65\ n_{GW}$, $\nu_i^*$,

$\nu_e^* \geq 1.2$. Which of these parameters, if any, is critical has to be established by further experimental parameter variation, in particular wider scans of $q_{95}$ at different plasma current. There seems to be no upper limit on density; with pellet fueling $n = 1.5 \times n_{\mathrm{GW}}$ has been reached, limited only by the pellet injector capacity [11]. Below the minimum density, ELM suppression or significant mitigation has not been found so far in ASDEX Upgrade, despite these plasmas having dimensionless parameters in the range reported by DIII-D [10]. However, the perturbation field seems to influence particle transport, resembling the "density pump-out" observed, e.g. in MAST [12]. An experimental next step will be the installation of another eight in-vessel coils, allowing us to the use of $n = 4$ perturbations. This upgrade is also useful to further study $n = 2$ fields, since the amplitude of the $n = 2$ component can be increased by a factor of $\sqrt{2}$ and the resonance condition can be tested at finer steps of $q_{95}$.

## Acknowledgement

M Willensdorfer is a fellow of the Friedrich Schiedel Foundation of Energy Technology.

## References

[1] A. Loarte, G. Saibene, R. Sartori, D. Campbell, M. Bécoulet, L. Horton, T. Eich, A. Herrmann, G. Matthews, N. Asakura, et al., Plasma Phys. Control. Fusion 45 (2003) 1549.
[2] G. Federici, Physica Scripta T124 (2006) 1.
[3] T. C. Hender, R. Fitzpatrick, A. W. Morris, P. G. Carolan, R. D. Durst, T. Edlington, J. Ferreira, S. J. Fielding, P. S. Haynes, J. Hugill, et al., Nucl. Fusion 32 (1992) 2091.
[4] T. E. Evans, R. A. Moyer, P. R. Thomas, J. G. Watkins, T. H. Osborne, J. A. Boedo, E. J. Doyle, M. E. Fenstermacher, K. H. Finken, R. J. Groebner, et al., Phys. Rev. Lett. 92 (2004) 235003.
[5] T. E. Evans, R. A. Moyer, J. G. Watkins, T. H. Osborne, P. R. Thomas, M. Bécoulet, J. A. Boedo, E. J. Doyle, M. E. Fenstermacher, K. H. Finken, et al., Nucl. Fusion 45 (2005) 595.
[6] W. Suttrop, A. Herrmann, M. Rott, T. Vierle, U. Seidel, B. Streibl, D. Yadikin, O. Neubauer, B. Unterberg, E. Gaio, et al., Fusion Eng. Design 84 (2009) 290, and references therein.
[7] W. Suttrop et al., Phys. Rev. Lett. 206 (2011) 225004.
[8] R. Fischer et al., in *Europhysics Conference Abstracts (CD-ROM), Proc. of the 38th EPS Conference on Controlled Fusion and Plasma Physics, Strasbourg, France, 2011*, volume xxx, Geneva, 2011, EPS, P1.072.
[9] M. Greenwald et al., Nucl. Fusion 28 (1988) 2199.
[10] T. E. Evans, M. E. Fenstermacher, R. A. Moyer, T. H. Osborne, and J. G. Watkins, Nuclear fusion 48 (2008).
[11] P. T. Lang et al., in *Europhysics Conference Abstracts (CD-ROM), Proc. of the 38th EPS Conference on Controlled Fusion and Plasma Physics, Strasbourg, France, 2011*, volume xxx, Geneva, 2011, EPS, Py.yyy.
[12] A. Kirk, Y. Liu, E. Nardon, P. Tamain, and P. Cahyna, Plasma Physics and Controlled Fusion 53 (2011).